coatings

MDPI

Article

Enhanced Transmittance Modulation of SiO_2-Doped Crystalline WO_3 Films Prepared from a Polyethylene Oxide (PEO) Template

Guanguang Zhang, Kuankuan Lu, Xiaochen Zhang, Weijian Yuan, Honglong Ning *, Ruiqiang Tao, Xianzhe Liu, Rihui Yao * and Junbiao Peng

Institute of Polymer Optoelectronic Materials and Devices, State Key Laboratory of Luminescent Materials and Devices, South China University of Technology, Guangzhou 510640, China;
msgg-zhang@mail.scut.edu.cn (G.Z.); mskk-lu@mail.scut.edu.cn (K.L.); mszhang_xc@mail.scut.edu.cn (X.Z.); 201430320366@mail.scut.edu.cn (W.Y.); 201510102158@mail.scut.edu.cn (R.T.); msliuxianzhe@mail.scut.edu.cn (X.L.); psjbpeng@scut.edu.cn (J.P.)
* Correspondence: ninghl@scut.edu.cn (H.N.); yaorihui@scut.edu.cn (R.Y.); Tel.: +86-20-8711-4525 (H.N.)

Received: 26 May 2018; Accepted: 23 June 2018; Published: 26 June 2018

Abstract: Polyethylene oxide (PEO)-modified silicon dioxide (SiO_2)-doped crystalline tungsten trioxide (WO_3) films for use as electrochromic layers were prepared on indium tin oxide (ITO) glass by the sol–gel spin coating technique. The effects of the PEO template and SiO_2 on the electrochromic transmittance modulation ability of crystalline WO_3 films were investigated. Fourier transform infrared spectroscopy (FT-IR) spectra analysis indicated that PEO was decomposed after annealing at 500 °C for 3 h. X-ray diffraction (XRD) pattern analysis showed that both SiO_2 and PEO helped reduce the crystalline grain size of the WO_3 films. Atomic force microscope (AFM) images showed that the combined action of SiO_2 and PEO was helpful for achieving high surface roughness and a macroporous structure. An electrochromic test indicated that PEO-modified SiO_2-doped crystalline WO_3 films intercalated more charges (0.0165 C/cm^2) than pure WO_3 crystalline films (0.0095 C/cm^2). The above effects resulted in a good transmittance modulation ability (63.2% at 628 nm) of PEO-modified SiO_2-doped crystalline WO_3 films, which was higher than that of pure WO_3 crystalline films (9.4% at 628 nm).

Keywords: tungsten trioxide; crystalline film; doping; morphology; electrochromism; transmittance modulation

1. Introduction

Tungsten trioxide (WO_3) is an important functional material, widely studied for applications in gas sensors [1], photochromism [2], photocatalysis [3], and electrochromism [4]. In recent years, the energy consumption of buildings for indoor temperature regulation has been increasing. Smart windows can reduce energy consumption by modulating light and heat inputs [5]. WO_3-based electrochromic layers have attracted increasing attention for smart windows applications. There are many methods for preparing WO_3 films, such as physical vapor deposition (PVD) [6], chemical vapor deposition (CVD) [7], sol–gel method [8], etc. However, both PVD and CVD have some characteristic drawbacks, such as high cost of equipment, high energy consumption, and vacuum dependency [9]. The sol–gel method can form large-area films in the atmosphere with less energy consumption and low equipment cost [10]. It is easy to realize doping uniformly at the molecular level by the sol–gel method. In addition, the pores formed by solvent evaporation during annealing can enhance the electrochromic properties of the films [11].

The electrochromic performance of WO_3 has been researched for several decades. As we know, the electrochromic performance is closely related to the morphology, structure, and crystallinity of the WO_3 films, and one effective method for enhancing the films' electrochromic performance is to incorporate dopants such as TiO_2 [12], Fe_2O_3 [13], carbon [14], etc. It was found that crystalline WO_3 films have good redox stability [15], good durability [16], and good infrared-reflecting properties (good insulation) [17]. However, compared with amorphous WO_3 films, a drawback of crystalline WO_3 films is their low transmittance modulation ability [18,19], which limits their application.

To enhance the electrochromic performance, especially the transmittance modulation ability of crystalline WO_3 films, a feasible scheme is to develop large-surface area and macroporous crystalline WO_3 films. In previous studies, polyethylene oxide (PEO) was often used as a template for pore materials [20]. SiO_2 has been confirmed to help form pores [21] and reduce the crystalline grain size [22]. In our work, we tried to improve the transmittance modulation ability of crystalline WO_3 films by combining the advantages of PEO and SiO_2. As a result, we successfully prepared crystalline pure WO_3 films, SiO_2-doped crystalline WO_3 films, PEO-modified crystalline WO_3 films, and PEO-modified SiO_2-doped crystalline films by the sol–gel method. Besides, the FT-IR spectra, crystallization, surface morphology, and electrochromic properties of these films were investigated.

2. Materials and Methods

Tungsten powder (purity: 99.5%) and hydrogen peroxide (mass fraction: 30%) were mixed in a beaker (weight: 4 g, H_2O_2: 20 mL) to prepare a tungstate solution. When the tungsten powder completely reacted, the tungstate solution was condensed into 10 mL by heating, in order to remove superfluous H_2O_2. Next, four kinds of solution were prepared, as shown in Table 1. Solution EW (pure tungstate solution) was a control solution, and solutions EWS (with SiO_2), EWP (with PEO), EWPS (with SiO_2 and PEO) were experimental solutions. The tungstate solution concentration was around 1 mol/L. According to a previous study [22], a concentration of tetraethyl orthosilicate (TEOS) of 0.2 mol/L had a good inhibitory effect. PEO amounts had a significant effect on the structure and quality of the WO_3 films. In this experiment, the amounts of the above reactants were optimized and controlled for the control experiment. After stirring and heating, the four kinds of sol were obtained, as shown in Figure 1. All of them were transparent, colloid (Tyndall effect), and orange-yellow, which indicated that PEO and TEOS were uniformly dissolved in the sol.

Table 1. The parameters of four kinds of solution. EW, control solution, pure tungstate solution; EWS, EWP, EWPS, experimental solutions (with SiO_2, PEO, SiO_2 and PEO, respectively).

Label	Absolute Ethanol/mL	Tungstate Solution/mL	Tetraethyl Orthosilicate (TEOS)/g	PEO polyethylene Oxide (M_w: 600,000)/g	Stirring Time/h	Heating Temperature/°C
EW	2.5	2.5	0	0	3	70
EWS	2.5	2.5	0.21	0		
EWP	2.5	2.5	0	0.1		
EWPS	2.5	2.5	0.21	0.1		

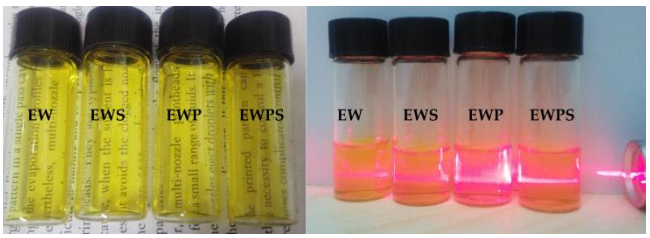

Figure 1. Images of sols of EW, EWS, EWP, and EWPS. All of them are transparent, colloid (Tyndall effect), and orange-yellow, which indicates that PEO and TEOS were uniformly dissolved in the sol.

Finally, all the films were prepared on ITO glass by spin coating (4000 revolutions per minute for 30 s). The area of the electrochromic layer was around 2 cm^2. The pure WO_3 films, SiO_2-doped WO_3 films, PEO-modified WO_3 films, and PEO-modified SiO_2-doped films annealed at 500 °C were named EW500, EWS500, EWP500, and EWPS500, respectively. Similarly, the PEO-modified SiO_2-doped films annealed at 100 and 300 °C were named EWPS100 and EWPS300, respectively.

The thickness of all films was measured by a probe surface profiler (Veeco Dektak 150, Veeco, NY, USA) and was about 200 ± 10 nm. FT-IR spectra of EWPS100, EWPS300, and EWPS500 were recorded by a FT-IR spectrophotometer (SHIMADZU IR Prestige-21, SHIMADZU, Tokyo, Japan) with an ITO glass acting as a blank. The crystalline structure of these films was determined by X-ray Diffraction using Cu Kα radiation (XRD, PANalytical Empyrean DY1577, PANalytical, Almelo, Netherlands). The surface morphology was measured by atomic force microscopy (AFM, Being Nano-Instruments BY3000, Being Nano-Instruments, Beijing, China). An amount of 0.8 mol/L of lithium perchlorate/propylene carbonate ($LiClO_4$/PC) electrolyte was used for the electrochromic test, and the electrode gap was 0.5 cm. The voltage supply and current measurement were supported by an electrochemical workstation (CH Instruments CHI600E, CH Instruments, Shanghai, China). The transmittance of these films at the initial state, colored state, and bleached state was measured by a spectrometer (Morpho PG2000, Morpho, Shanghai, China) with an ITO glass acting as blank.

3. Results and Discussion

Figure 2 shows the changes of the appearance of the EW500, EWS500, EWP500, and EWPS500 films as the annealing time increased. Because of the carbonization of PEO at high temperature, it indicates that the color of samples EWP500 and EWPS500 (PEO-doped) changed from transparent to grey after annealing for 15 min, when compared with EW500 and EWS500 (not PEO-doped), but such changes did not occur in samples EW500 and EWS500, because of the rapid evaporation of the organic solvents. Finally, the color of samples EWP500 and EWPS500 turned transparent again as the annealing time increased. In the process of PEO pyrolysis, CO_2 and water vapor, which acted on the film structure, escaped from the WO_3 film.

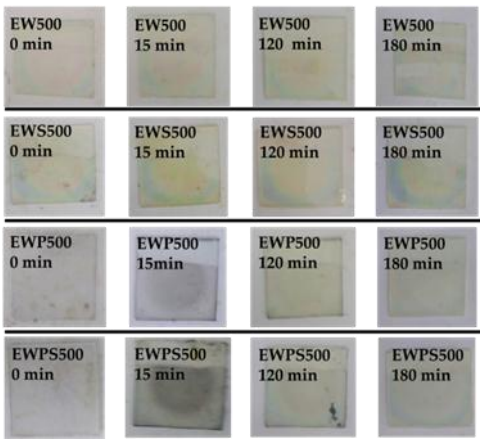

Figure 2. Changes of the appearance of the EW500, EWS500, EWP500, and EWPS500 films (annealed at 500 °C) as the annealing time increased. The color changed from transparent to grey and finally turned transparent again only in the samples EWP and EWPS (PEO-doped), which indicated the carbonization of PEO at high temperature.

Figure 3 shows the FT-IR spectra of EWPS100, EWPS300, and EWPS500, which were annealed at different temperatures. The spectra (a), (b), and (c) of Figure 3 show broad bands located at 3500–3400 cm^{-1}, which were attributed to asymmetric and symmetric –OH stretching vibrations. In addition, another

sharp band around 1625 cm^{-1} was attributed to –OH bending vibration [23]. The –OH was mainly from physisorbed water and surface OH groups.

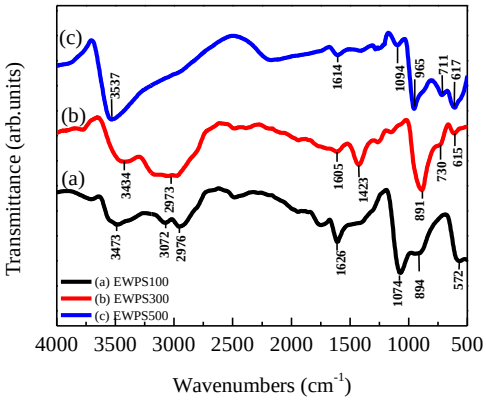

Figure 3. Fourier transform infrared (FT-IR) spectra of EWPS films: (**a**) EWPS100 (annealed at 100 °C); (**b**) EWPS300 (annealed at 300 °C); (**c**) EWPS500. The annealing process at 500 °C led to PEO pyrolysis and formation of W–O–W and Si–O–Si structures.

As spectra (a) and (b) of Figure 3 show, the bands located around 2900–3000 cm^{-1} correspond to the symmetric and antisymmetric –C–H stretching vibration of aliphatic CH_3 and CH_2 from ethanol and PEO [24]. The bands located around 3000–3100 cm^{-1} correspond to symmetric and antisymmetric =C–H stretching vibration, which was attributed to incomplete pyrolysis of PEO [25]. The bands around 1423 cm^{-1} could be assigned to asymmetric –C–H bending vibration [26]. In spectrum (a), the sharp band around 1074 cm^{-1} could be assigned to the asymmetric C–O–C stretching vibration from PEO [26]. In spectrum (a), the bands at 894 and 572 cm^{-1} were attributed to symmetric and antisymmetric $W(O)_2$ stretching vibration and O–O stretching vibration, respectively [27]. In spectra (b) and (c), the bands around 965 cm^{-1} were attributed to symmetric W=O stretching vibration, and the bands at 615 and 730 cm^{-1} were attributed to asymmetric W–O–W stretching vibration [27,28]. The bands around 1094 cm^{-1} were attributed to asymmetric Si–O–Si stretching vibration in spectrum (c) [29].

Therefore, the above FT-IR spectra analysis indicated that the organic components, including PEO and ethanol, were strongly reduced after film annealing at 500 °C for 3 h. PEO was decomposed into CO_2 and H_2O which play a significant role in the formation of large surface area and macroporous structures. Besides, the annealing process led to the formation of W–O–W and Si–O–Si structures.

Figure 4 shows the XRD patterns of EW500, EWS500, EWP500, EWPS500, and ITO glass, which were analyzed using the software Jade 6.0 and PDF #43-1035. As Figure 4 shows, the diffraction peaks of WO_3 could be observed in the patterns (a), (b), (c), and (d), which indicated that all these WO_3 films were crystallized. The main peak of WO_3 at $2\theta \approx 24.1°$ corresponds to the (200) planes, and its crystalline grain size was calculated using the Scherrer formula [30]:

$$D = \frac{0.89\gamma}{\beta \cos \theta} \quad (1)$$

where D is the average size of the grain on the (200) plane, γ is the X-ray wavelength, which is 0.154056 nm, β is the full width at half maximum (FWHM) of the diffraction peak, θ is the diffraction angle. The grain sizes of these films are shown in Figure 5; the smallest grain size was found in the sample EWPS500. The results indicated that both the PEO and SiO_2 dopants are helpful for reducing the grain size; a smaller grain size indicates that there are more grain boundaries and defects in the films. Further, the XRD patterns in Figure 4 also indicated that the diffraction peak of SiO_2 resulted from the ITO glass rather than the SiO_2 dopant. SiO_2 is amorphous and is present at the grain

boundaries [31,32], inhibiting the continuous growth of the grains; therefore, the grain sizes of samples EWPS500 and EWS500 were smaller than that of sample EW500.

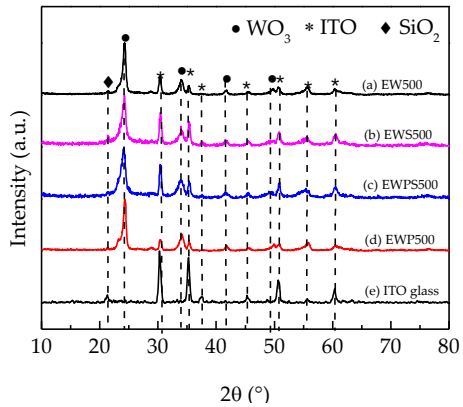

Figure 4. X-ray diffraction (XRD) patterns of different films: (**a**) EW500; (**b**) EWS500; (**c**) EWP500; (**d**) EWPS500; (**e**) indium tin oxide (ITO) glass. All of them were crystallized by annealing at 500 °C.

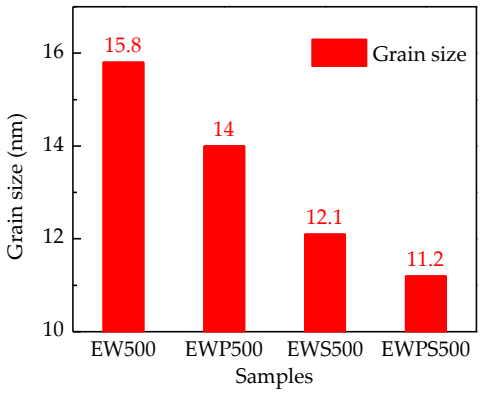

Figure 5. Crystalline grain sizes of different WO_3 films, calculated using the WO_3 main peaks ($2\theta \approx 24.1°$) in the XRD patterns.

Figures 6 and 7 show the AFM 3D images (10,000 nm × 10,000 nm) of four kinds of samples and the surface roughness and increased surface area (ΔS, compared with their projected area: 10,000 nm × 10,000 nm) of these samples, respectively. In Figure 6, it indicates that in samples EWP500 and EWPS500 (PEO-doped), the macroporous structure is large compared with samples EW500 and EWS500 (not PEO-doped), which indicated that the PEO template plays an important role in the formation of a rough surface and a macroporous structure, because PEO was decomposed into CO_2 and H_2O when annealing was carried out at 500 °C for 3 h. Figure 7 indicates that the SiO_2 dopant also helped to increase the roughness compared with the control film EW500. The surface area of all the experimental films was larger than that of the control film, and sample EWPS500 showed the best result. In this material system, the SiO_2 dopant cooperated with PEO to inhibit grain growth and increase surface roughness and surface area.

Figure 8 shows the current curves of different WO_3 films in a cycle of electrochromic test under ±2 V voltages. The injecting and extracting charges per unit area (ΔQ) were calculated on the basis of the current of a cycle of electrochromic test. As we know, the electrochromic mechanism refers to a process of Li^+ and electron migration [33]:

$$WO_3(\text{colorless}) + xe^- + xLi^+ \rightarrow Li_xWO_3(\text{Blue}) \quad (2)$$

Li^+ is the main charge carrier in the $LiClO_4$/PC electrolyte. The above process finishes when the currents tend to 0 mA. Among the four samples, the ΔQ of sample EW500 were the least, which indicated that there was a low amount of Li_xWO_3 generated in sample EW500. The time corresponding to 90% of the total current change is defined as the electrochromic response time. In Figure 8, all films show a short electrochromic response time (around 7 s), which is acceptable and closed to a normal level [34].

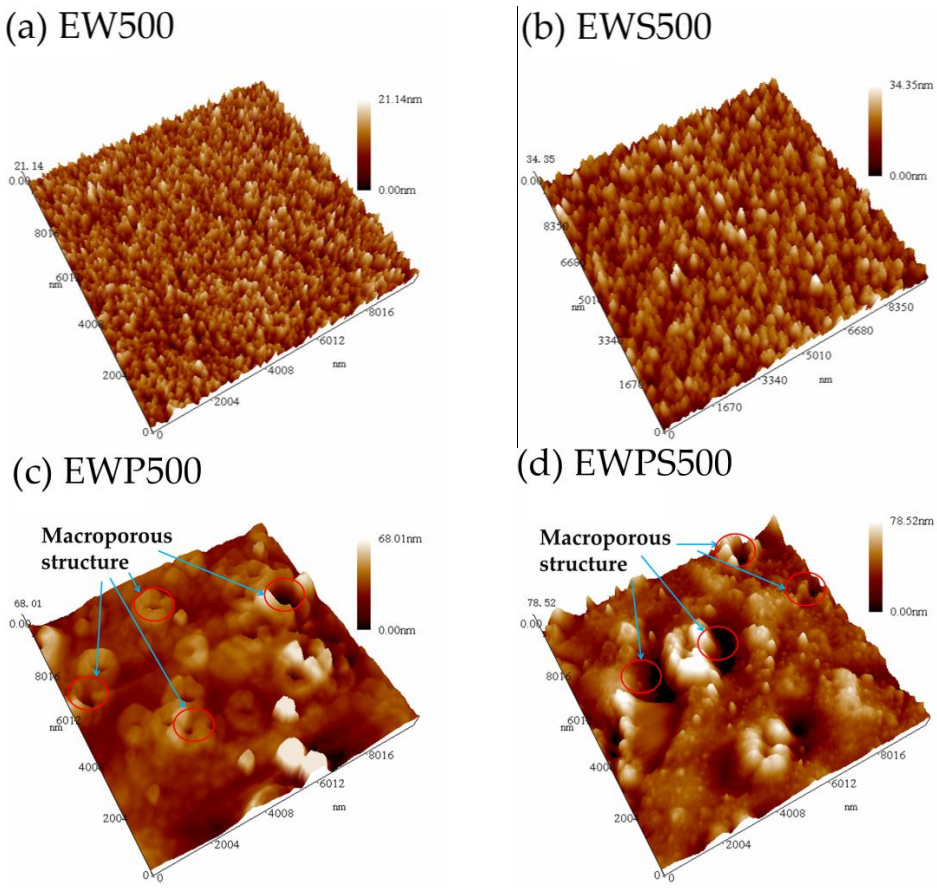

Figure 6. Atomic force microscope (AFM) 3D images (10,000 nm × 10,000 nm) of different WO_3 films: (**a**) EW500, (**b**) EWS500,(**c**) EWP500, (**d**) EWPS500.

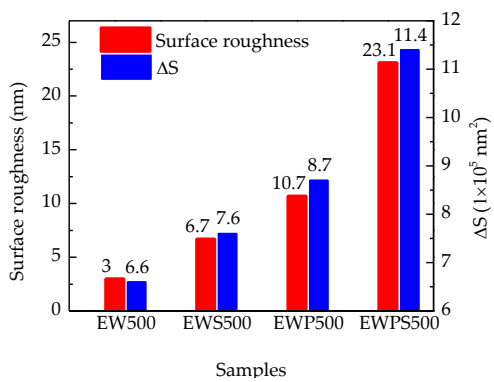

Figure 7. The surface roughness and increased surface area (ΔS, compared with their projected area: 10,000 nm × 10,000 nm) of EW500, EWS500, EWP500, and EWPS500, which were determined from the corresponding AFM images by the AFM support software.

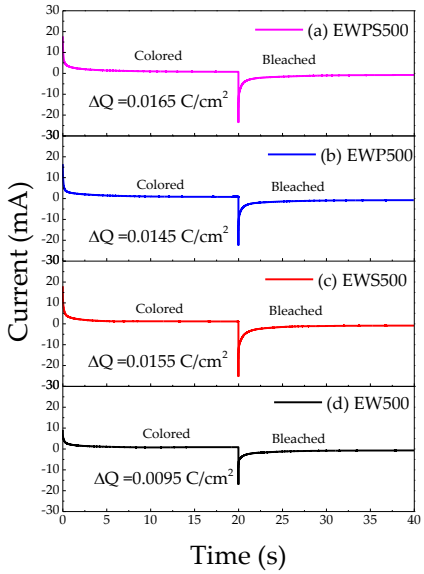

Figure 8. The current curves of different WO_3 films in a cycle of electrochromic test under ±2V voltages: (**a**) EWPS500; (**b**) EWP500; (**c**) EWS500; (**d**) EW500.

Both the images and the transmittance of the initial state, colored state, and bleached state of these samples are shown in Figure 9. The transmittance modulation ability (ΔT) is defined by the following formula at wavelength 628 nm:

$$\Delta T = |T_c - T_b| \tag{3}$$

In this formula, T_c and T_b are the transmittance of the colored state and bleached state at wavelength 628 nm, respectively. ΔT directly shows the optical contrasts in a certain percentage. In this experiment, the ITO glass (substrate) was used as a blank, whose transmittance was designated as 100% in the wavelength range of 400–900 nm. According to Figure 9, the ΔT of these samples were calculated, and the results were 9.4% (EW500), 27.8% (EWS500), 35.5% (EWP500), and 63.2% (EWPS500). It indicates that the ΔT of sample EWPS500, whose color was deep blue at the color state, was the highest among these samples. This indicates that sample EWPS500 could effectively reduce the passing of light.

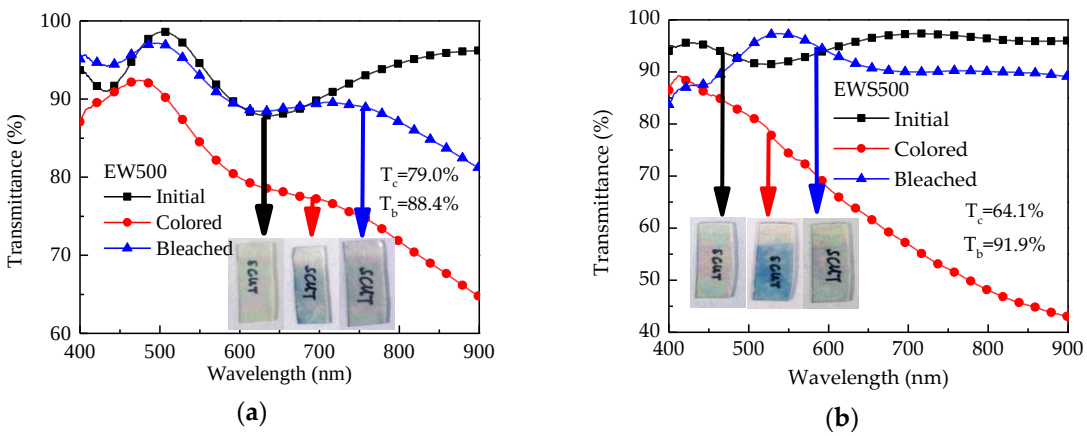

Figure 9. *Cont.*

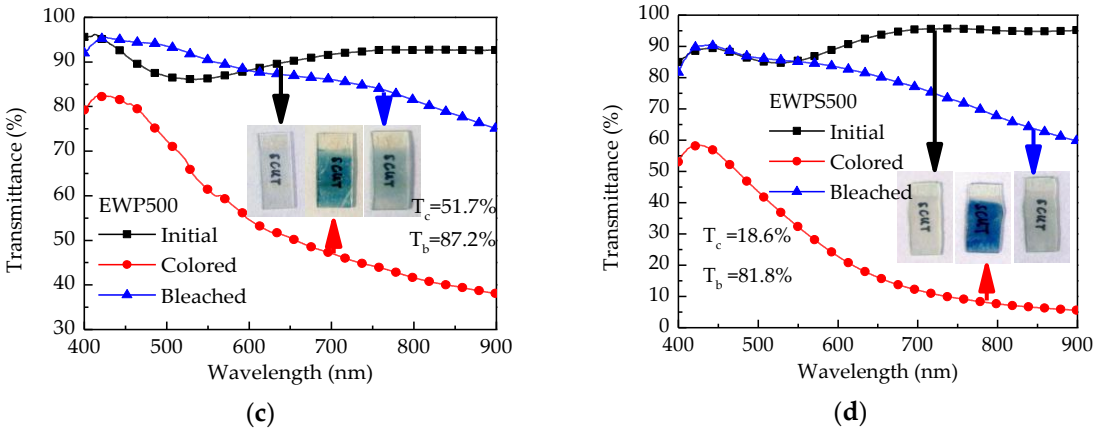

Figure 9. The transmittance and images of different WO_3 films at the initial state, colored state, and bleached state: (**a**) EW500; (**b**) EWS500; (**c**) EWP500; (**d**) EWPS500. T_c and T_b are the transmittance of the colored state and bleached state at wavelength 628 nm, respectively.

In addition, coloration efficiency (CE) is another important parameter for evaluating the electrochromic performance, defined by the following formula [35,36]:

$$\mathrm{CE} = \frac{\Delta \mathrm{OD}}{\Delta Q} = \frac{\ln \frac{T_b}{T_c}}{\Delta Q} \tag{4}$$

In Formula (4), ΔOD is the optical density; ΔQ, T_c, and T_b were defined above. Figure 10 shows the different CE of the four samples. There was an increase in the CE of the WO_3 crystalline films when PEO and SiO_2 were used as the dopants. Both PEO and SiO_2 were efficient in enhancing the electrochromic performance, but the combined use of SiO_2 and PEO could further increase the CE from 23.23 cm^2/C (EWS500) or 35.86 cm^2/C (EWP500) to 89.69 cm^2/C (EWPS500). Figure 11 shows the different ΔT of the first and the 500th cycle. It indicates that the transmittance modulation changed little (within 5%). Therefore, all four samples showed stable cycle characteristics, which is an advantage of the crystalline WO_3 films [15,16].

It is worth comparing the electrochromic transmittance modulation ability in our work with the past reported data. Table 2 shows these comparisons. The results showed that the modulation ability of the crystalline WO_3 film was enhanced successfully by PEO modification and SiO_2 doping compared with other crystalline WO_3 films. Further, the transmittance modulation ability of EWPS500 appeared as good as that of the amorphous WO_3 film.

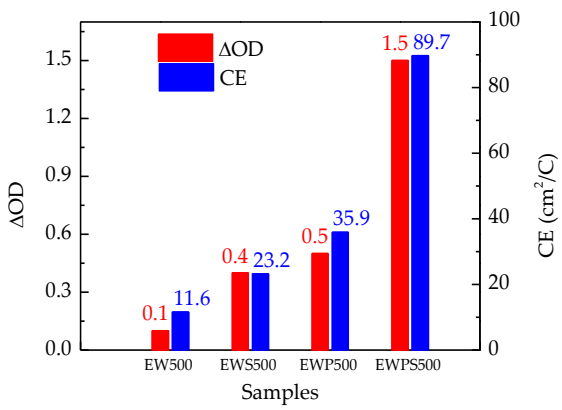

Figure 10. The optical density (ΔOD) and coloration efficiency (CE) of samples EW500, EWS500, EWP500 and EWPS500.

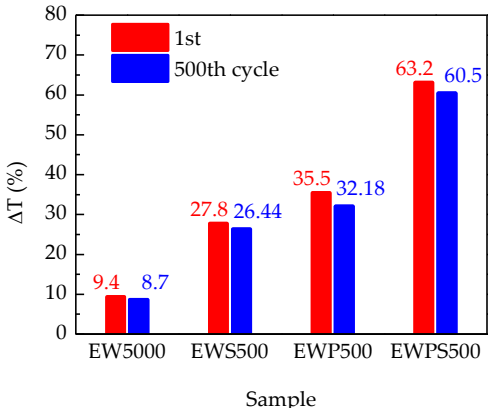

Figure 11. The transmittance modulation ability (ΔT at 628 nm) with ±2 V voltages at the 1st and 500th cycle. The ΔT of these crystalline WO_3 films changed within 5%.

Table 2. Comparisons with the past reported data: Electrochromic film, synthetic method, crystallinity, and ΔT at 628 nm.

Electrochromic Film	Synthetic Method	Crystallinity	ΔT at 628 nm	Reference
EWPS500	Sol–gel method	Crystalline	63.2%	This work
PEG400 doped WO_3	Sol–gel method	Crystalline	~14%	[19]
WO_3	Thermal evaporation	Crystalline	~32%	[36]
WO_3	Thermal evaporation	Amorphous	~66%	[36]
2%V_2O_5 doped WO_3	RF magnetron sputtering	Amorphous	~49%	[37]

As mentioned above, the electrochromic performance is closely related to the morphology, structure, and crystallinity of the WO_3 films. The PEO template was decomposed into CO_2 and H_2O after annealing at 500 °C, which resulted in a high surface roughness and a macroporous structure. The high surface roughness indicated that there was a large surface area for reaction. Meanwhile, the pores on the structure provide channels for $LiClO_4$/PC electrolyte, so Li^+ can easily enter the internal structure. Therefore, both EWP500 and EWPS500 showed better electrochromic transmittance modulation ability than EW500 and EWS500. In addition, the SiO_2 dopant could further increase the surface roughness, so the electrochromic transmittance modulation ability of EWPS500 was enhanced to the highest levels, compared with that of other samples. However, the influence of crystallinity cannot be ignored. As we know, the component of the grain boundaries is amorphous WO_3, which contains multiple defects. Li^+ is easily intercalated into these defects, generating blue Li_xWO_3. The XRD analysis indicated that SiO_2 could inhibit the growth of the grains effectively, and the most direct proof of this phenomenon was the decrease of the grain size, which indicated that the grain boundaries were larger in samples EWS50, EWP500, and EWPS500. Sample EWPS500 had the above characteristics, so its transmittance modulation ability was the most outstanding among these samples.

4. Conclusions

PEO-modified and SiO_2-doped crystalline WO_3 films were prepared by the sol–gel spin coating technique. The combined action of PEO and SiO_2 increased the surface roughness and formed a macroporous structure on the films. In addition, both PEO and SiO_2 could reduce the crystalline grain size effectively. The above characteristics of morphology, structure, and crystallinity resulted in a good electrochromic transmittance modulation of the crystalline WO_3 films. The PEO-modified and SiO_2-doped crystalline WO_3 films could intercalate more charges (0.0165 C/cm^2) than the pure WO_3

films (0.0095 C/cm^2). Moreover, the transmittance modulation ability (ΔT = 63.2% at 628 nm) of the former films was better than that of the latter films (ΔT = 9.4% at 628 nm).

Author Contributions: Conceptualization, G.Z.; Formal analysis, G.Z.; Funding acquisition, H.N., R.Y., and J.P.; Investigation, G.Z., X.Z., and W.Y.; Methodology, G.Z.; Project administration, H.N., R.Y., and J.P.; Supervision, H.N.; Writing—original draft, G.Z.; Writing—review & editing, K.L., H.N., R.T., X.L., R.Y., and J.P.

Funding: This work was supported by the National Key R&D Program of China (2016YFB0401504), National Natural Science Foundation of China (51771074, 51521002 and U1601651), National Key Basic Research and Development Program of China (973 program, 2015CB655004) Founded by MOST, Guangdong Natural Science Foundation (2016A030313459 and 2017A030310028), Guangdong Science and Technology Project (2016B090907001, 2016A040403037, 2016B090906002, 2017B090907016 and 2017A050503002), Guangzhou Science and Technology Project (201804020033).

Acknowledgments: We thank Jingxin Qin for her linguistic assistance during the preparation of this manuscript.

Conflicts of Interest: The authors declare no conflict of interest.

References

1. Shendage, S.S.; Patil, V.L.; Vanalakar, S.A.; Patil, S.P.; Harale, N.S.; Bhosale, J.L.; Kim, J.H.; Patil, P.S. Sensitive and selective NO_2 gas sensor based on WO_3 nanoplates. *Actuators B Chem.* **2017**, *240*, 426–433. [CrossRef]
2. Miyazaki, H.; Ishigaki, T.; Suzuki, H.; Ota, T. Effect of film thickness and air atmosphere on photochromic properties of WO_3-based composite films. *Bull. Chem. Soc. Jpn.* **2016**, *89*, 20–23. [CrossRef]
3. Sotelo-Vazquez, C.; Quesada-Cabrera, R.; Ling, M.; Scanlon, D.O.; Kafizas, A.; Thakur, P.K.; Lee, T.L.; Taylor, A.; Watson, G.W.; Palgrave, R.G.; et al. Evidence and effect of photogenerated charge transfer for enhanced photocatalysis in WO_3/TiO_2 heterojunction films: A computational and experimental study. *Adv. Funct. Mater.* **2017**, *27*, 1605413. [CrossRef]
4. Granqvist, C.G. Electrochromic tungsten oxide films: Review of progress 1993–1998. *Sol. Energy Mater. Sol. Cells* **2000**, *60*, 201–262. [CrossRef]
5. Wang, Y.; Runnerstrom, E.L.; Milliron, D.J. Switchable materials for smart windows. *Annu. Rev. Chem. Biomol. Eng.* **2016**, *7*, 283–304. [CrossRef] [PubMed]
6. Esmail, A.; Hashem, H.; Soltan, S.; Hammam, M.; Ramadan, A. Thickness dependence of electro-optical properties of WO_3 films as an electrochromic functional material for energy-efficient applications. *Phys. Status Solidi A* **2017**, *214*, 1600478-10. [CrossRef]
7. Vernardou, D.; Psifis, K.; Louloudakis, D.; Papadimitropoulos, G.; Davazoglou, D.; Katsarakis, N.; Koudoumas, E. Low pressure CVD of electrochromic WO_3 at 400 °C. *J. Electrochem. Soc.* **2015**, *162*, H579–H582. [CrossRef]
8. Sahu, D.R.; Hung, C.Y.; Wang, S.C.; Huang, J.L. Existence of electrochromic reversibility at the 1000th cyclic voltammetry for spin coating WO_3 film. *Ionics* **2017**, *23*, 3227–3233. [CrossRef]
9. Garg, D.; Henderson, P.B.; Hollingsworth, R.E.; Jensen, D.G. An economic analysis of the deposition of electrochromic WO_3 via sputtering or plasma enhanced chemical vapor deposition. *Mater. Sci. Eng. B Adv. Funct. Solid-State Mater.* **2005**, *119*, 224–231. [CrossRef]
10. Myzelev, A. Electrochromic properties of sol-gel synthesized macroporous tungsten oxide films doped with gold nanoparticles. *J. Electrochem. Soc.* **2014**, *161*, H276–H283.
11. Cheng, W.; Baudrin, E.; Dunn, B.; Zink, J.I. Synthesis and electrochromic properties of mesoporous tungsten oxide. *J. Mater. Chem.* **2000**, *11*, 92–97. [CrossRef]
12. Zhan, Y.; Tan, M.R.J.; Cheng, X.; Tan, W.M.A.; Cai, G.F.; Chen, J.W.; Kumar, V.; Magdassi, S.; Lee, P.S. Ti-doped WO_3 synthesized by a facile wet bath method for improved electrochromism. *J. Mater. Chem. C* **2017**, *5*, 9995–10000. [CrossRef]
13. Azimirad, R.; Akhavan, O.; Moshfegh, A.Z. An investigation on electrochromic properties of $(WO_3)_{1-x}$–$(Fe_2O_3)_x$ thin films. *Thin Solid Films* **2006**, *515*, 644–647. [CrossRef]
14. Lee, C.T.; Chiang, D.; Chiu, P.K.; Chang, C.M. WO_3 electrochromic thin films doped with carbon. *IEEE Trans. Magn.* **2014**, *50*, 3501204. [CrossRef]
15. Zhou, D.; Xie, D.; Shi, F.; Wang, D.H.; Ge, X.; Xia, X.H.; Wang, X.L.; Gu, C.D.; Tu, J.P. Crystalline/amorphous tungsten oxide core/shell hierarchical structures and their synergistic effect for optical modulation. *J. Colloid Interface Sci.* **2015**, *460*, 200–208. [CrossRef] [PubMed]

16. Chu, J.; Lan, J.; Lu, D.; Ma, J.; Wang, X.; Wu, B.; Gong, M.; Zhang, R.; Xiong, S. Facile fabrication of WO_3 crystalline nanoplate on FTO glass and their application in electrochromism. *Micro Nano Lett.* **2016**, *11*, 749–752. [CrossRef]
17. Hutchins, M.G.; Butt, N.S.; Topping, A.J.; Gallego, J.; Milne, P.; Jeffrey, D.; Brotherston, I. Infrared reflectance modulation in tungsten oxide based electrochromic devices. *Electrochim. Acta* **2001**, *46*, 1983–1988. [CrossRef]
18. Zhao, B.; Zhang, X.; Dong, G.; Wang, H.; Yan, H. Efficient electrochromic device based on sol–gel prepared WO_3 films. *Ionics* **2015**, *21*, 2879–2887. [CrossRef]
19. Li, Y.J.; Liu, Z.F.; Liang, X.P.; Ya, J.; Cui, T.; Liu, Z.C. Synthesis and electrochromic properties of PEG doped WO_3 film. *Mater. Technol.* **2014**, *29*, 341–349. [CrossRef]
20. Liang, C.; Dai, S. Dual phase separation for synthesis of bimodal meso-/macroporous carbon monoliths. *Chem. Mater.* **2009**, *21*, 2115–2124. [CrossRef]
21. Li, D.; Wu, G.; Gao, G.; Shen, J.; Huang, F. Ultrafast coloring-bleaching performance of nanoporous WO_3–SiO_2 gasochromic films doped with Pd catalyst. *ACS Appl. Mater. Interfaces* **2011**, *3*, 4573–4579. [CrossRef] [PubMed]
22. Righettoni, M.; Tricoli, A.; Pratsinis, S.E. Thermally stable, silica-doped ε-WO_3 for sensing of acetone in the human breath. *Chem. Mater.* **2010**, *22*, 3152–3157. [CrossRef]
23. Gerand, B.; Nowogrocki, G.; Figlarz, M. A new tungsten trioxide hydrate, $WO_3 \cdot {}^1/_3H_2O$: Preparation, characterization, and crystallographic study. *J. Solid State Chem.* **1981**, *38*, 312–320. [CrossRef]
24. Guo, C.; Liu, H.Z.; Wang, J.; Chen, J.Y. Conformational structure of triblock copolymers by FT-Raman and FTIR spectroscopy. *J. Colloid Interface Sci.* **1999**, *209*, 368–373. [CrossRef] [PubMed]
25. Finocchio, E.; Cristiani, C.; Dotelli, G.; Stampino, P.G.; Zampori, L. Thermal evolution of PEG-based and BRIJ-based hybrid organo-inorganic materials. FT-IR studies. *Vib. Spectrosc.* **2014**, *71*, 47–56. [CrossRef]
26. Wen, S.J.; Richardson, T.J.; Ghantous, D.I.; Striebel, K.A.; Ross, P.N.; Cairns, E.J. FTIR PEO + $LiN(CF_3SO_2)_2$ electrolytes. *J. Electroanal. Chem.* **1996**, *408*, 113–118. [CrossRef]
27. Deepa, M.; Sharma, N.; Varshney, P.; Varma, S.P.; Agnihotry, S.A. FTIR investigations of solid precursor materials for sol-gel deposition of WO_3 based electrochromic films. *J. Mater. Sci.* **2000**, *35*, 5313–5318. [CrossRef]
28. Rougier, A.; Portemer, F.; Quédé, A.; Marssi, M.E. Characterization of pulsed laser deposited WO_3 thin films for electrochromic devices. *Appl. Surf. Sci.* **1999**, *153*, 1–9. [CrossRef]
29. López, T.; Tzompantzi, F.; Hernández-Ventura, J.; Gómez, R.; Bokhimi, X.; Pecchi, G.; Reyes, P. Effect of zirconia precursor on the properties of ZrO_2-SiO_2 sol-gel oxides. *J. Sol-Gel Sci. Technol.* **2002**, *24*, 207–219. [CrossRef]
30. Ramkumar, S.; Rajarajan, G. Effect of Fe doping on structural, optical and photocatalytic activity of WO_3 nanostructured thin films. *J. Mater. Sci. Mater. Electron.* **2016**, *27*, 1847–1853. [CrossRef]
31. Zeng, X.; Zhou, Y.; Ji, S.; Luo, H.; Yao, H.; Huang, X.; Jin, P. The preparation of a high performance near-infrared shielding Cs_xWO_3/SiO_2 composite resin coating and research on its optical stability under ultraviolet illumination. *J. Mater. Chem. C* **2015**, *3*, 8050–8060. [CrossRef]
32. Gao, G.; Feng, W.; Wu, G.; Shen, J.; Zhang, Z.; Jin, X.; Zhang, Z.; Du, A. An investigation on the assembling of WO_3 particles on the matrix of silica solution. *J. Sol-Gel Sci. Technol.* **2012**, *64*, 427–435. [CrossRef]
33. Haro-Poniatowski, E.; Jouanne, M.; Morhange, J.F.; Julien, C.; Diamant, R.; Fernández-Guasti, M.; Fuentes, G.A.; Alonso, J.C. Micro-Raman characterization of WO_3 and MoO_3 thin films obtained by pulsed laser irradiation. *Appl. Surf. Sci.* **1998**, *127–129*, 674–678. [CrossRef]
34. Najafi-Ashtiani, H.; Bahari, A.; Ghasemi, S. A dual electrochromic film based on nanocomposite of copolymer and WO_3 nanoparticles: Enhanced electrochromic coloration efficiency and switching response. *J. Electroanal. Chem.* **2016**, *774*, 14–21. [CrossRef]
35. Camirand, H.; Baloukas, B.; Klemberg-Sapieha, J.E.; Martinu, L. In situ spectroscopic ellipsometry of electrochromic amorphous tungsten oxide films. *Sol. Energy Mater. Sol. Cells* **2015**, *140*, 77–85. [CrossRef]

36. El-Nahass, M.M.; Saadeldin, M.M.; Ali, H.A.M.; Zaghllol, M. Electrochromic properties of amorphous and crystalline WO_3 thin films prepared by thermal evaporation technique. *Mater. Sci. Semicond. Process.* **2015**, *29*, 201–205. [CrossRef]
37. Meenakshi, M.; Gowthami, V.; Perumal, P.; Sivakumar, R.; Sanjeeviraja, C. Influence of dopant concentration on the electrochromic properties of tungsten oxide thin films. *Electrochim. Acta* **2015**, *174*, 302–314.